VIBRATION-BASED DAMAGE DETECTION IN A WIND TURBINE BLADE BASED ON AUTOREGRESSIVE COEFFICIENTS

S. Hoell & P. Omenzetter, *The LRF Centre for Safety and Reliability Engineering, The University of Aberdeen, UK*

ABSTRACT

Wind energy is at the forefront of renewable energy harvesting. Thus, the increasing interest in renewable energy in the European Union [1] leads to growing sizes of wind turbines (WTs) and erections in remote areas, such as offshore. The application of structural health monitoring in structural components of WTs offers an attractive opportunity to optimise operational costs and to increase safety and reliability. Different techniques have been developed for structural damage detection (SDD) in WTs. However, the majority are not suitable for in-service measurements or require very dense sensor arrays. This paper presents a vibration-based SDD method applied to a numerical WT blade (WTB) model with a shear-web disbonding damage scenario. The damage sensitive feature (DSF) is developed as the Mahalanobis distance between a baseline and a current vector of autoregressive coefficients (ARCs) estimated from acceleration response time series. The acceleration signals are obtained from transient dynamic simulations of numerical WTB models with a simplified aerodynamic loading approach. First, conventional time series modelling, i.e. model order selection and parameter validation, is presented. Second, sensitivities of ARCs for increasing damage extents and an ARC selection for damage detection are discussed. Third, the SDD results based on statistical hypothesis testing are assessed for different sets of ARCs with respect to the detectability of early damage. This enabled to demonstrate the challenges of ARC-based SDD with respect to the detection of early damages. The numerical simulations conducted demonstrate the sensitivity of the proposed ARC-based DSF, which is promising for future developments of SDD methods in WTs.

NOMENCLATURE

ACF	Autocorrelation Function
AIC	Akaike Information Criterion
AR	Autoregressive
ARC	Autoregressive Coefficient
ARMA	Autoregressive Moving Average
DOF	Degree of Freedom
DSF	Damage Sensitive Feature
FE	Finite Element
NREL	National Renewable Energy Laboratory
SDD	Structural Damage Detection
SNL	Sandia National Laboratory
WT	Wind Turbine
WTB	Wind Turbine Blade

1. INTRODUCTION

Due to the promotion of renewable energy by the European Union's energy policy [1], efficient wind energy harvesting becomes increasingly important. The consequences are growing sizes of WTs and erections in remote areas, such as offshore. This leads to increasing operation and maintenance costs, which can make up to 20% of the total energy production costs [2]. Efficient structural health monitoring systems can counteract the increase in operation and maintenance costs. Furthermore, the safety and reliability of WTs can be improved.

SDD in WTBs deserves special attention because up to 19.4% of WT failure incidents were caused by blade damages [3]. However, currently available methods for continuous monitoring of the structural state of WTBs, such as acoustic emission and strain monitoring [4], are local methods. To monitor complex structures, very dense sensor arrays are required, thus instrumentation and data analysis are costly.

Under the premise that damage leads to changes of stiffness, mass or energy dissipation mechanisms of a structure [5], vibration response signals can be used to define DSFs which describe the current, healthy or damaged, structural state. Modal parameters, such as natural frequencies, modal damping ratios or mode shapes, as well as non-parametric and parametric time series representations can be utilized for vibration-based SDD [6].

The method discussed in this paper is based on parametric time series models obtained from acceleration response signals. Autoregressive moving average (ARMA) models were utilized for SDD by Carden and Brownjohn [7]. They showed theoretical connections between parametric model orders and the number of observable modes of physical structures. However, due to the invertibility property of autoregressive (AR) and moving average processes [8], AR models can be used instead of ARMA models to describe the underlying process. Nair et al [9] demonstrated theoretically the relationship between structural stiffness and ARCs.

A unified statistical framework for time series-based structural health monitoring has been presented by Fassois and Sakellariou [10], where statistical hypothesis testing of ARC-based DSFs, as applied in the present paper, is one case. Choosing the appropriate AR model order is a crucial step of this method. The influence of autoregressive model orders on SDD results was discussed by Figueiredo et al. [11]. They found that AR models of conventionally estimated orders enable to detect damage.

This paper discusses the influence of ARC selection for SDD in a WTB with emphasis on early damage detection, where coefficients are selected from conventionally identified AR models. The following section gives a detailed description of the theory related to AR-based SDD. Then, numerical simulations of a single WTB are presented. This includes a simplified aerodynamic loading approach and a selected disbonding damage scenario. The parametric modelling and SDD results are shown in the following section. Finally, a discussion of the results and prospects for the future work are given in the final section before rounding up the paper with a set of conclusions.

2. THEORY

Time invariant AR models can only be used for stationary processes, thus it is assumed that the vibration response signals of the healthy and damaged structure are stationary. Performing a normalization of the initial signals enables to account for loading variability, e.g. due to varying wind speeds in the present case. This can be done for a time series by removing the estimated mean and dividing by the estimated standard deviation.

2.1 TIME SERIES MODELLING

For an AR(p) process of order p, a current value of a time series $z[t]$ at time instant t can be expressed as the weighted sum of p previous values and a noise term $e[t]$:

$$z[t] = a_1 z[t-1] + \ldots + a_p z[t-p] + e[t] \qquad (1)$$

where the system unknowns are the ARCs, a_i i=1,…p, and the variance σ_e^2 of the normally distributed, independent, random noise term. The Burg algorithm [12] is used in this study to estimate the unknowns.

However, prior to the estimation, the selection of an appropriate model order is required. The selected order should enable to capture the underlying system dynamics while being computationally efficient. The Akaike information criterion (AIC) is commonly used for the selection of AR orders, which evaluates the models based on the model likelihood. The sample number normalized AIC can be calculated with the estimated noise variances, $\hat{\sigma}_e^2$, as [8]:

$$AIC(p) = \ln(\hat{\sigma}_e^2) + \frac{2(p+1)}{n} \qquad (2)$$

where n is the number of samples, and the hat denotes estimated quantities. The first term refers to the model likelihood, while the second is a penalty for the model complexity.

Similar to the model order selection, the validation of estimated models is generally required to assure the model adequacy. This is usually done by examining the residuals, which can be obtained by modifying Eq. (1) as follows:

$$\hat{e}[t] = z[t] - \hat{a}_1 z[t-1] - \ldots - \hat{a}_p z[t-p] \qquad (3)$$

To test the residuals as a whole, the residual autocorrelations, r_e, and a test statistic can be employed. The modified Ljung-Box-Pierce

statistic, Q, [8] is used herein and can be defined as:

$$Q = n(n+2)\sum_{k=1}^{K}\frac{r_e^2[k]}{(n-k)} \tag{4}$$

The unbiased k-th coefficient of the autocorrelation function (ACF) can be calculated with [13]:

$$r_e[k] = \frac{1}{n-k}\sum_{i=1}^{n-k} e[i]e[i+k] \tag{5}$$

For a valid model, the test statistic Q follows a $\mathcal{X}^2$ distribution with $K-p$ degrees of freedom (DOFs). This can be utilized to define a statistical hypothesis test in order to validate an appropriate AR model.

2.2 STATISTICAL HYPOTHESIS TESTING

In the present paper, the SDD phase employs a statistical hypothesis testing approach. The estimated DSF vectors, $\hat{\mathbf{v}}$, are generally constructed for selected AR model orders p as

$$\hat{\mathbf{v}} = \begin{bmatrix} \hat{a}_1 & \hat{a}_2 & \cdots & \hat{a}_p \end{bmatrix}^T \tag{6}$$

where superscript T denotes transpose. It is assumed that the single vector entries are independent of each other and Gaussian distributed. Thus, the difference $\Delta\hat{\mathbf{v}}$ between the estimated DSF vectors of the healthy structure and the current structure, $\hat{\mathbf{v}}_h$ and $\hat{\mathbf{v}}_c$, follows a multivariate Gaussian distribution, $\mathcal{N}(\boldsymbol{\mu}_{\Delta\mathbf{v}}, \boldsymbol{\Sigma}_{\Delta\mathbf{v}})$:

$$\Delta\hat{\mathbf{v}} = \hat{\mathbf{v}}_c - \hat{\mathbf{v}}_h \sim \mathcal{N}(\boldsymbol{\mu}_{\Delta\mathbf{v}}, \boldsymbol{\Sigma}_{\Delta\mathbf{v}}) \tag{7}$$

with the true mean, $\boldsymbol{\mu}_{\Delta\mathbf{v}}$, given as the difference between the true DSF vectors of the healthy and the current structure as

$$\boldsymbol{\mu}_{\Delta\mathbf{v}} = \mathbf{v}_c - \mathbf{v}_h \tag{8}$$

and the true variance-covariance matrix, $\boldsymbol{\Sigma}_{\Delta\mathbf{v}}$, as

$$\boldsymbol{\Sigma}_{\Delta\mathbf{v}} = \boldsymbol{\Sigma}_h + \boldsymbol{\Sigma}_c \tag{9}$$

where $\boldsymbol{\Sigma}_h$ and $\boldsymbol{\Sigma}_c$ are the true variance-covariance matrices of the healthy and current state, respectively.

However, if the structure is healthy then the difference follows a zero-mean multivariate Gaussian distribution with variance-covariance $\boldsymbol{\Sigma}_{\Delta\mathbf{v}} = 2\boldsymbol{\Sigma}_h$. In this case, the squared Mahalanobis distance, D^2, defined as

$$D^2 = \Delta\hat{\mathbf{v}}^T\boldsymbol{\Sigma}_{\Delta\mathbf{v}}^{-1}\Delta\hat{\mathbf{v}} \sim \mathcal{X}_m^2 \tag{10}$$

follows, as a squared sum of independent Gaussian variables, a central $\mathcal{X}^2$ distribution with m DOFs, $\mathcal{X}_m^2$. The true variance-covariance matrix is generally unavailable, thus the estimated version $\hat{\boldsymbol{\Sigma}}_{\Delta\mathbf{v}}$ is used instead. The DOFs correspond to the DSF vector dimensionality.

The hypothesis testing problem can be defined as

$$\begin{aligned} H_0: &\quad \Delta\mathbf{v} = \mathbf{v}_c - \mathbf{v}_h = \mathbf{0} \quad (\textit{healthy}) \\ H_1: &\quad \Delta\mathbf{v} = \mathbf{v}_c - \mathbf{v}_h \neq \mathbf{0} \quad (\textit{damaged}) \end{aligned} \tag{11}$$

where the null hypothesis, H_0, describes the healthy state and the alternative hypothesis, H_1, the damaged state. This enables to define a statistical test of the squared Mahalanobis distance by means of the cumulative $\mathcal{X}^2$ distribution function, $F_{\mathcal{X}_m^2}$, as

$$\begin{aligned} D^2 < F_{\mathcal{X}_m^2}(1-\alpha) &\Rightarrow H_0 \text{ is accepted} \\ \text{Else} &\Rightarrow H_0 \text{ is rejected} \end{aligned} \tag{12}$$

where α is the selected level of significance.

2.3 AR COEFFICIENT SELECTION FOR DAMAGE SENSITIVE FEATURE

The ARCs are generally differently affected by damage, or have different sensitivities to damage. It is important to select them for inclusions in the DSF in such a way that only these that help the most to detect damage in early stages are retained because the thresholds of multivariate statistics, used for damage hypothesis testing, such as $F_{\mathcal{X}_m^2}$, will also increase with the number of statistical DOFs for a given significance level. Therefore, the aim is to identify the number of ARCs below which their contribution to the detectability of damage outpaces the growth of the statistical threshold, as this will give the most conclusive distinction between the healthy and the damage states.

In the present paper, a two-step approach is proposed for the selection of ARCs. First, the coefficients are ranked with respect to their sensitivity to damage with the help of the Mahalanobis distance between coefficients from the healthy and one selected damage state. Second, the effect of the increasing number of ranked ARCs with respect to the corresponding threshold $F_{\mathcal{X}_m^2}(1-\alpha)$ at a selected level of significance is examined in order to identify the optimum number of the included coefficients.

Initial number of AR coefficients in set is p

FOR $j = 1$ to $p-1$

FOR $i = 1$ to n coefficients in set

1. Temporary removal of candidate coefficient a_i from set

$$\Delta\mathbf{v}_i = \begin{bmatrix} \vdots & \\ \bar{a}_{h,t-1} - \bar{a}_{d,t-1} \\ \bar{a}_{h,t-1} - \bar{a}_{d,t-1} \\ \vdots & \end{bmatrix} \quad \boldsymbol{\Sigma}_{\Delta v,t} = \begin{bmatrix} \ddots & \\ \sigma^2_{h,t-1i-1} & \sigma^2_{h,t-1i-1} \\ \sigma^2_{h,t-1i-1} & \sigma^2_{h,t-1i-1} \\ & \ddots \end{bmatrix}$$

2. Calculation of remaining Mahalanobis distance

$$D_i^2 = \Delta\hat{\mathbf{v}}_i^T \boldsymbol{\Sigma}_{\Delta v,i}^{-1} \Delta\hat{\mathbf{v}}_i$$

END

3. Permanent removal of candidate with highest remaining Mahalanobis distance from set

END

Figure 1: Ranking procedure for ARCs

The first part of the procedure uses a step-down algorithm to identify the coefficients that have the smallest contribution to the Mahalanobis distance for the selected damage. The algorithm is presented in Figure 1, where the subscript *d* refers to estimates from the damaged state. The sample mean of the ARCs is indicated by the bar. The initial, whole set of coefficients is incrementally reduced by the coefficient that gives the smallest contribution to the Mahalanobis distance until only one ARC is left. The ranking of ARCs is given by the inverse order in which they are removed. For example, the coefficient removed in the first iteration causes the smallest change of the Mahalanobis distance and has the lowest ranking.

In the second step, Mahalanobis distances are calculated for increasing numbers of ARCs with highest rankings. The results are divided by the threshold value given by the cumulative distribution $F_{\chi^2_m}(1-\alpha)$ at a selected level of significance α. The number of DOFs, m, corresponds to the number of included ARCs retained. The maximum of that ratio the optimum number of coefficients.

Even though this approach takes the multivariate statistics of coefficients into account, it eliminates the coefficients one by one. However, strictly speaking the true optimal selection can only be found by considering all possible $2^p - 1$ selections of ARCs, but that would be computationally prohibitive.

3. SIMULATIONS

The structure under study is a numerical model of a large WTB. An ANSYS Mechanical [14] finite element (FE) model of a single cantilevered blade was created with the help of the Sandia National Laboratory (SNL), USA, software package NuMAD [15] and the specifications of the SNL's 61.5 m reference WTB [16]. These specifications are based on the National Renewable Energy Laboratory (NREL), USA, 5 MW reference WT design [17]. A baseline FE model with 1,650 SHELL281 elements was found adequate by element type and mesh size studies.

Transient dynamic simulations are performed to generate response acceleration time series. For the assessment of vibration-based SDD methods, the realistic simulation of excitations is important, thus a simplified aerodynamic loading approach is developed. The simulations are done for a single WTB, where a parked WT situation is assumed and tower motions are ignored.

Aerodynamic loads are obtained in three steps. First, the NREL software TurbSim [18] is used to generate full-field wind data according to the international standard IEC 61400-1, 3rd Edition [19]. The mean wind speed at the hub height is selected to be 10 m/s, which is the average wind speed of an IEC Type I WT. The resulting turbulence intensity of the inflow wind component is 18.34% for the wind category B and the normal turbulence model.

In the second step, aerodynamic loads are calculated with the NREL software packages AeroDyn [20] and FAST [21], where the wake effect is modelled by the blade element momentum theory. The WTB is therefore approximated by 17 strip elements, each of constant aerodynamic and structural properties. Time series of lift and drag forces, and pitching moments at the element centres are the result.

The third step is a mapping of these element loads to nodal forces of the surface nodes in the FE model. This procedure is based on Berg et al. [22]. Equilibrium equations of forces and moments for each WTB element enable to establish a linear system of equations, which can be solved numerically. Since the mapping is generally not-unique, non-zero pitching moments in y-direction and linear spatial distributions are chosen. This procedure enables to calculate load

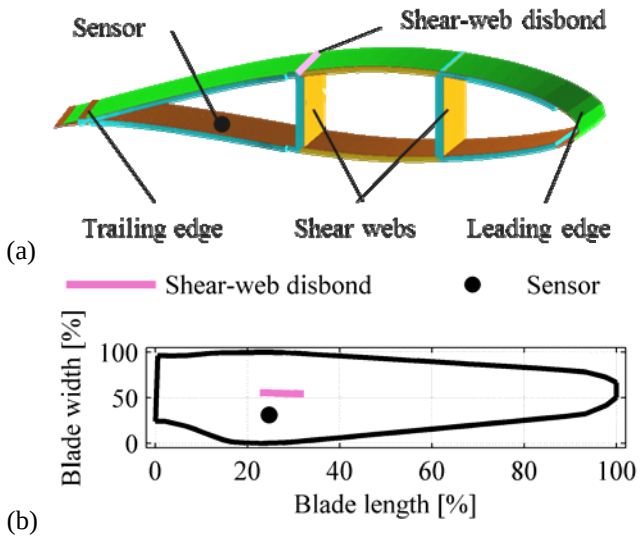

Figure 2: Damage and sensor location in WTB; (a) cross section, (b) top view

coefficients for nodal forces of each surface node, thus during the transient dynamic simulations only simple evaluations are required for every load step. The simulations are performed with a constant time step of 0.005 s.

Transient simulations are not only performed for the healthy baseline WTB model but also for FE models of damaged WTBs. Disbonding of one shear-web from the low pressure cap is selected as damage scenario, see Figure 2. Jensen et al. [23] performed a full scale structural test on a 34 m long WTB until failure for flap-wise bending. They observed a disbonding of the outer skin from the load-carrying box girder, which is herein simulated as shear-web disbonding. From real inspections [24], the maximum chord location is found to be damage prone, therefore it is chosen as initial damage location with extension towards the WTB's tip. The disbonding is introduced in the FE model with a separation of nodes between elements at selected locations. The damage extent, and with it, the length of the disbonding correspond to the number of separated nodes.

4. RESULTS

The effect of shear-disbonding is assessed by means of numerical modal analysis for the healthy and the damaged WTB FE models. The maximum disbonding extent is chosen to be approx. 6.2 m or 10.2% of the WTB length. The relative difference Δf_i between the natural frequencies of the healthy $f_{h,i}$ and the damaged model $f_{d,i}$ gives the effect of damage on the i-th frequency as

$$\Delta f_i = (f_{h,i} - f_{d,i}) / f_{h,i} \times 100\% \quad (13)$$

Figure 3a shows these effects for the first ten natural frequencies, where contributions of the first and second frequency are invisible due to their minor changes. Further, it can be seen that the cumulative sum of relative frequency differences and the disbond length have a nonlinear relationship. The highest contributions to the sum are from modes 5 and 10 with frequencies of the healthy WTB of 5.55 Hz and 12.72 Hz, respectively. Furthermore, the wind speed amplitude spectrum of the inflow wind

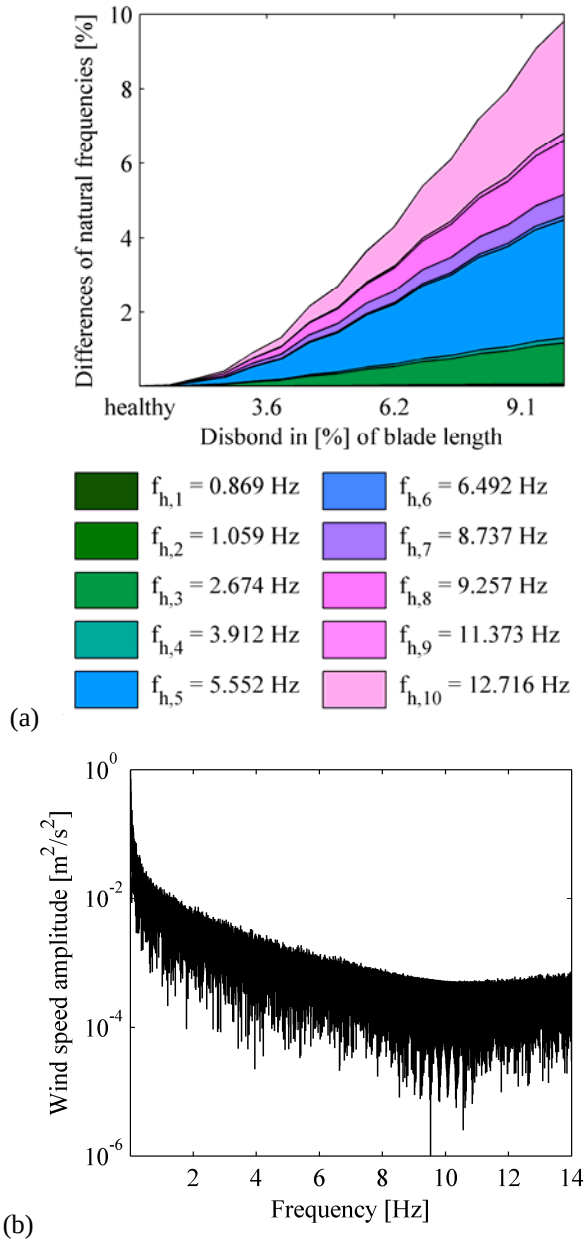

Figure 3: (a) Cumulative relative differences of natural frequencies with increasing shear-web disbonding; (b) Wind speed amplitude spectrum for simulated inflow wind component

component at the hub position is given as reference for the aerodynamic excitation in Figure 3b. The realization of the inflow wind component is simulated with TurbSim for 630s based on the Kaimal spectrum and mean wind speed of 10 m/s. The Kaimal spectrum adopted has a low frequency excitation characteristic, which is important with respect to the changes in the natural frequencies due to damage. It can be noticed that the significant changes of mode 10 will have only a minor contribution to the damage detectability as this mode will be weakly excited. Only modes with frequencies less than 8 Hz can be assumed to be sufficiently excited to affect the damage detectability. This means for a disbond of 6.2% of the WTB length the cumulative relative frequency difference is only 2%, which illustrates the challenge of vibration-based SDD for this structure.

For the following discussion of AR modelling and SDD, transient dynamic simulations are performed for the healthy and damaged WTB FE models. Flap-wise and edge-wise accelerations at selected nodes are obtained for a durations of 630 s. Only flap-wise signals for the node indicated as 'Sensor' in Figure 2 are used in the following. Each time series is divided into 200 segments of 6,000 samples with a shift of 600 samples. The time series segments are initially low-pass filtered with a Chebyshev Type I filter and then decimated from 200 Hz to 25 Hz. In order to account for variations of the aerodynamic excitation, each pre-processed segment is normalised by its estimated mean and standard deviation.

The baseline phase of AR-based SDD uses data from the healthy structure to estimate the model parameters and to develop a statistical model for them. This requires initially the selection of an appropriate model order. Given in Eq. (2), the AIC is widely used to indicate an appropriate order for parametric time series modelling. Therefore, the AIC is calculated for all AR orders from one to 50, and shown in Figure 4. The mean and standard deviations of AIC values are calculated from the set of time series segments. The AIC indicates an AR model order of 25 because higher orders do not significantly improve the results. Therefore, the order of 25 is selected for the following investigations.

Complementary to the task of model order selection is model validation. This is shown here for one time series segment. The residuals, as given in Eq. (3), are tested for normal, independent and identical distribution. First, Figure 5a shows the residual's cumulative probability plot, where a straight line indicates a normal distribution. It can be seen that this is only violated at the tails. Second, the ACF of the residuals is shown in Figure 5b. Only four coefficients, or 1.6%, are out of the 95% bounds of a white noise process. Third, the modified Ljung-Box-Pierce statistics, as given in Eq. (4), are calculated for a selected numbers of

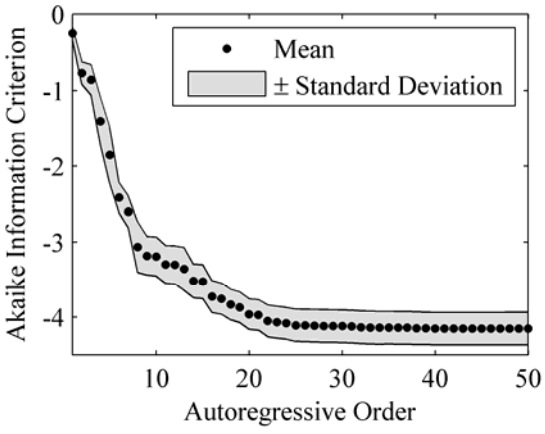

Figure 4: Mean and standard deviation of AICs for AR models of time series segments

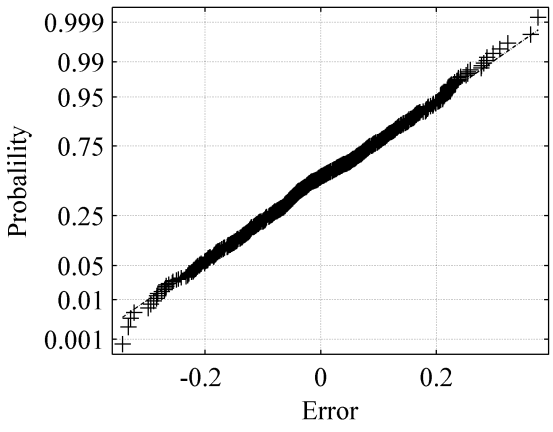

(a)

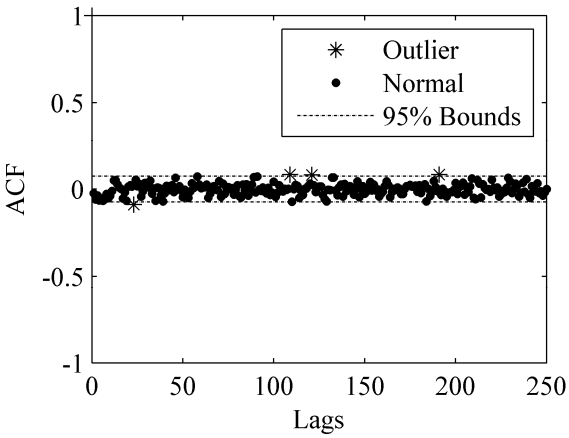

(b)

Figure 5: Validation of AR(25) model; (a) normality plot of residuals, (b) ACF of residuals

autocorrelation coefficients. From this test and the previous investigations, it is concluded that the appropriateness of the selected AR model order is supported.

The effect of increasing damage extents on ARCs of the AR(25) model is shown in Figure 6. Mean and standard deviation of the coefficients are calculated from the estimates of the time series segments. Each subplot is scaled according to the individual ranges of the coefficients to the unit internal 0-1 in order to present comparable results. It can be seen that the mean of the majority of coefficients changes monotonically with increasing damage. Only coefficient a_3 is almost unaffected. The standard deviations do not show such a clear pattern. They increase, decrease or stay almost constant for different ARCs.

Nevertheless, for a reliable distinction between structural states, not only shifts in mean but also the corresponding variations are important. Therefore, a more detailed investigation is performed with the help of Fisher's criterion, FC, as a measure of the ARCs' damage sensitivities to damage. For a univariate two class problem, it can be defined as

$$FC(i) = \frac{\left(\bar{a}_{d,i} - \bar{a}_{h,i}\right)^2}{\sigma_{d,i}^2 + \sigma_{h,i}^2} \tag{14}$$

where i corresponds to the i-th ARC. It is assessed by its mean $\bar{a}$ and variance σ^2 from the healthy and the damage state, superscript h and d, respectively. The result is a dimensionless measure for the separability between structural states. It is calculated for all ARCs and damage extents. Figure 7 shows the results, where the 95% confidence bound of the $F_{\chi_1^2}(95\%)$ distribution with one DOF is given as a reference. Values above this threshold indicate the detectability of damage by only using the corresponding single coefficient. This illustrates the sensitivity of the ARCs for the selected damage scenario. It can be seen that the ARCs a_1 to a_5 and a_{21} to a_{25} show only small changes with increasing damage. Most sensitive are the ARCs a_6 to a_{20}. This enables to perform a manual selection of coefficients according to these sensitivities, where the selection is indicated by stars in Figure 7.

However, this measure is only univariate, thus no information about the inter-relationships between the coefficients is used. Therefore, the ranking procedure, as discussed in Section 2.3, is applied with coefficients obtained from the healthy state and with a disbond of 5.6% blade length. The ranking of each coefficient is additionally given in Figure 7, where one indicates the highest and 25 the lowest contribution to the Mahalanobis distance. In comparison to the univariate sensitivity, it can be seen that there is no clear relationship between the ranking and the FC results. This behaviour can be explained by dependencies between coefficients, which are not considered in the univariate analysis.

The second part of the proposed ARC selection procedure is illustrated in Figure 8. It shows the relative Mahalanobis distances for increasing numbers of ARCs according to their ranking. The relative Mahalanobis distance is defined as

$$\tilde{D}_m^2 = D_m^2 \big/ F_{\chi_m^2}(95\%) \tag{15}$$

where the initial Mahalanobis distance D_m^2 for the m dimensional DSF vector is divided by the threshold values of the corresponding cumulative distribution $F_{\chi_m^2}(95\%)$ with m DOFs at the selected five percent level of significance. A value of one, which is indicated by the dashed line, corresponds to the relative distance equal to the threshold. Relative distances above indicate the detectability of the selected damage of 5.6% blade length. It can be seen that the damage is detectable by using more than 15 ARCs with the best ranking. However, 17 ARCs with the highest ranking are selected for the statistical hypothesis testing.

Finally, SDD is performed with the help of statistical hypothesis testing for increasing damage extents. For comparison, this is done for the ranking-based and the manually selected sets of 17 ARCs. The results are given in Table 1. The statistical threshold is defined by the value $F_{\chi_{17}^2}(95\%)$. It can be seen that the ranking-based selection outperforms the manual selection with respect to the detectability of early damages. The former enables to detect disbonds of 5.6% blade length with high confidence, because the non-alarm rate is lower than the selected level of significance. The manually selected ARCs allow only detecting disbonds of 10.2% blade length.

5. CONCLUSIONS

The present paper showed the application of ARC-based DSFs and statistical hypothesis testing for

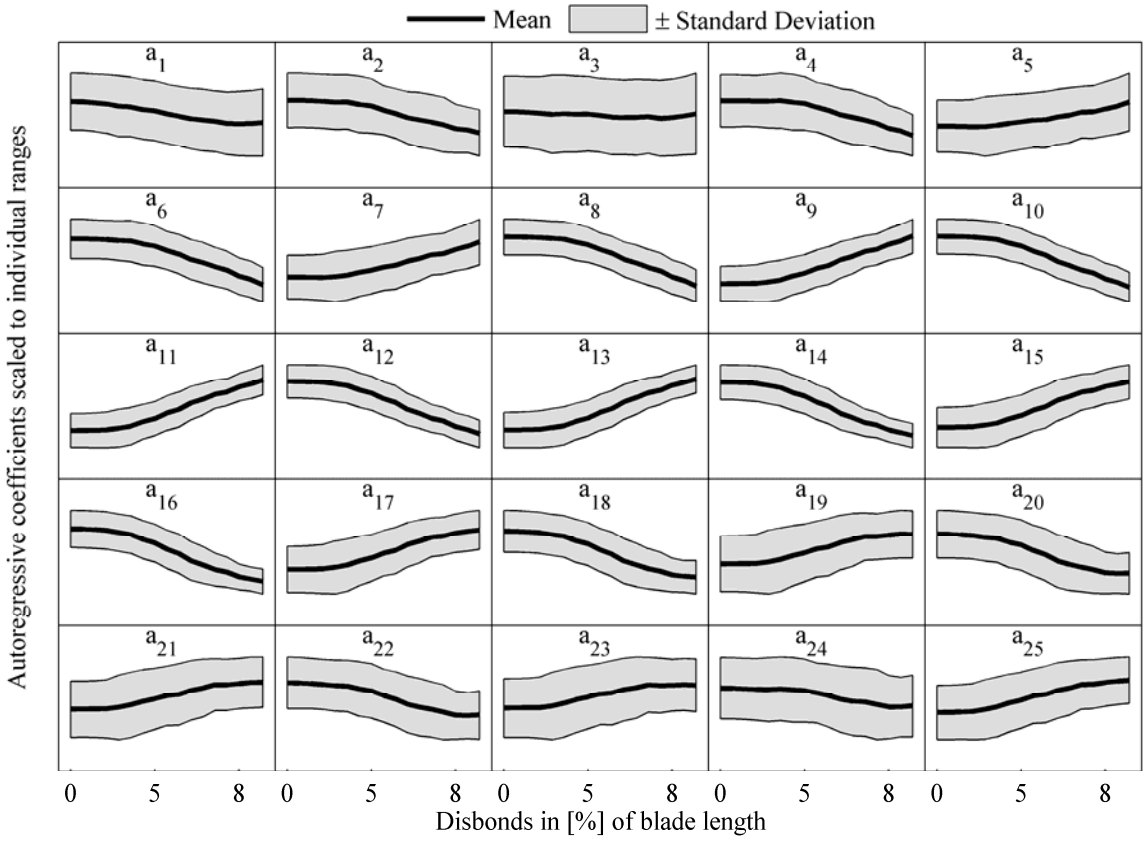

Figure 6: Mean and standard deviation of ARCs with increasing damage extents

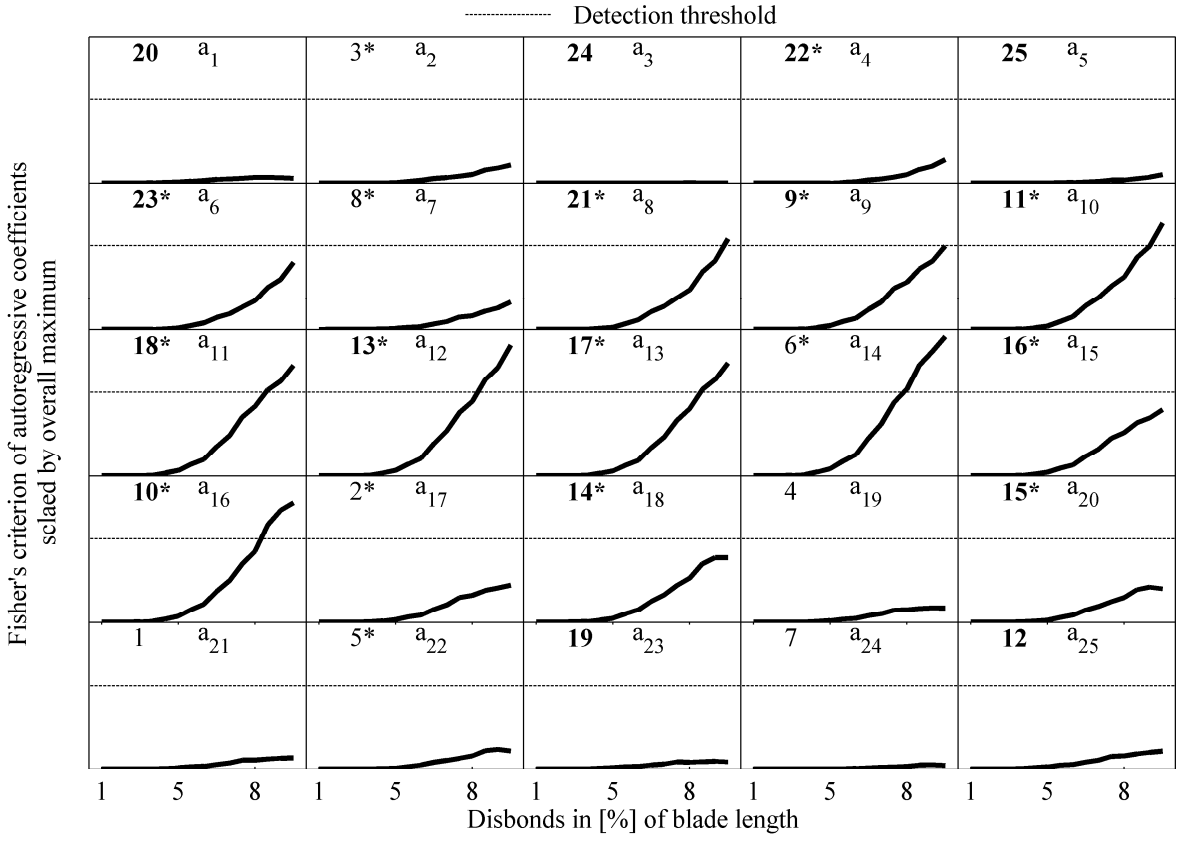

(b)

Figure 7: Fisher's criterion of ARCs with increasing damage and ARC ranking numbers; asterisks indicate manually selected coefficients, bold numbers indicate relative Mahalanobis ranking-based selection

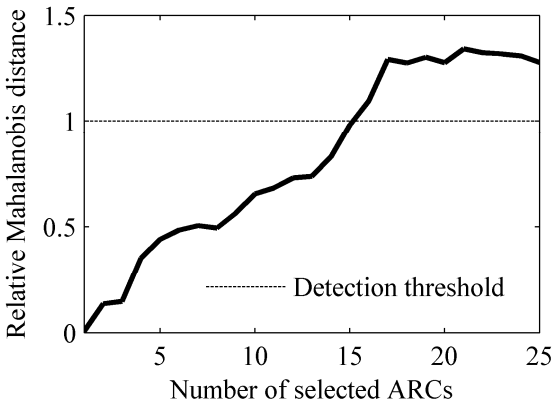

Figure 8: Relative Mahalanobis distance for increasing number of ranked ARCs

SDD in a large WTB. Damage decisions were obtained by Mahalanobis distances between vectors of ARCs estimated from acceleration response signals. Therefore, transient dynamic simulations were performed with a healthy FE WTB model and models with a shear-web disbonding damage scenario of several extents. To apply a realistic excitation, a simplified aerodynamic loading approach was developed, where blade element loads are mapped to nodal forces.

The results of conventional time series modelling, i.e. model order selection and model validation, are shown. Furthermore, the sensitivities of single ARCs to increasing damage extents were presented. The key aspect of the present paper was the discussion of the efficient selections of ARCs for early detection of shear-web disbonding in the numerical WTB model. Therefore, two different sets of ARCs were selected. One was manually selected with respect to the individual ARCs' sensitivities to damage. The other selection was done with a two-step approach including ARC ranking based on Mahalanobis distances and maximization of the damage detectability with respect to a statistical threshold.

Then, SDD was performed. In the baseline phase, ARCs were estimated to develop a statistical model for the DSF vectors of certain mean and variance-covariance according to the ARC selections. Statistical hypothesis testing by means of the Mahalanobis distances was employed in the detection phase to make decisions about the structural state of the current model. The relative rejection rates of the null hypothesis, which indicate the presence of damage, were used to illustrate the performance of the different ARC selection methods. The ranking-based ARC selection resulted in the smallest detectable disbonding of approx. 5.6% of the blade length outperforming the manual selection.

This study demonstrated the challenges of AR-based damage detection in a WTB with respect to the selection of coefficients. However, it was shown that ARCs as DSFs in a statistical hypothesis testing framework enable to detect shear-web disbonding of a moderate size. These findings are promising for future developments, although further research is required for the coefficient selection of parametric models in SDD using experimental studies.

Table 1: Relative rejection rates of H_0 in [%] as result of statistical hypothesis testing

Damage extent in [%] of blade length		Ranking-based selection	Manual selection
0.0	H_0	0.0	0.0
0.7	H_1	0.0	0.0
1.4	H_1	0.0	0.0
2.2	H_1	0.0	0.0
2.9	H_1	1.5	1.0
3.6	H_1	1.5	1.5
4.3	H_1	24.5	1.5
5.0	H_1	57.5	3.0
5.6	H_1	98.5	15.0
6.2	H_1	100.0	31.5
6.8	H_1	100.0	62.5
7.4	H_1	100.0	76.0
8.5	H_1	100.0	91.5
9.1	H_1	100.0	96.5
10.2	H_1	100.0	99.0

ACKNOWLEDGEMENTS

Piotr Omenzetter and Simon Hoell's work within the Lloyd's Register Foundation Centre for Safety and Reliability Engineering at the University of Aberdeen is supported by Lloyd's Register Foundation. The Foundation helps to protect life and property by supporting engineering-related education, public engagement and the application of research.

REFERENCES

1. THE EUROPEAN PARLIAMENT AND THE COUNCIL OF THE EUROPEAN UNION, 2009

‘The Renewable Energy Directive 2009/28/EC’, *Official Journal of the European Union, L 140.*
2. BLANCO MI,2009 ‘The Economics of Wind Energy’, *Renewable and Sustainable Energy Reviews, 13, 1372-82*.
3. CHOU JS, CHIU CK, HUANG IK, CHI KN,2013 ‘Failure Analysis of Wind Turbine Blade Under Critical Wind Loads’, *Engineering Failure Analysis, 27, 99-118.*
4. SCHUBEL PJ, CROSSLEY RJ, BOATENG EKG, HUTCHINSON JR,2013 ‘Review of Structural Health and Cure Monitoring Techniques for Large Wind Turbine Blades’, *Renewable Energy, 51, 113-23.*
5. FARRAR CR, WORDEN K,2007 ‘An Introduction to Structural Health Monitoring’, *Philosophical Transactions of the Royal Society A: Mathematical, Physical and Engineering Sciences, 365, 303-15.*
6. CARDEN EP, FANNING P,2004 ‘Vibration Based Condition Monitoring: A Review’, *Structural Health Monitoring, 3, 355-77.*
7. CARDEN EP, BROWNJOHN JMW,2008 ‘ARMA Modelled Time-Series Classification for Structural Health Monitoring of Civil Infrastructure’, *Mechanical Systems and Signal Processing, 22, 295-314.*
8. BOX GEP, JENKINS GM, REINSEL GC,2008 ‘Time Series Analysis Forecasting and Control’, *Hoboken, USA, John Wiley & Sons, Inc.*
9. NAIR KK, KIREMIDJIAN AS, LAW KH,2006 ‘Time Series-Based Damage Detection and Localization Algorithm with Application to the ASCE Benchmark Structure’, *Journal of Sound and Vibration, 291, 349-68.*
10. FASSOIS SD, SAKELLARIOU JS,2007 ‘Time-series Methods for Fault Detection and Identification in Vibrating Structures’, Philosophical Transactions of the Royal Society A: Mathematical, Physical and Engineering Sciences 2007; 365:411-48.
11. FIGUEIREDO E, FIGUEIRAS J, PARK G, FARRAR CR, WORDEN K,2011 ‘Influence of the Autoregressive Model Order on Damage Detection’, *Computer-Aided Civil and Infrastructure Engineering, 26, 225-38.*
12. KAY SM,1988 ‘Modern Spectral Estimation: Theory and Application’, *New Jersey, USA, Prentice Hall.*
13. BENDAT JS, PIERSOL AG,2010 ‘Random Data Analysis and Measurement Procedures’, *Hoboken, New Jersey, USA, John Wiley & Sons, Inc.*
14. SAS IP INC,2012 ‘ANSYS Mechanical APDL Theory Reference’.
15. BERG JC, RESOR BR,2012 ‘Numerical Manufacturing and Design Tool (NuMAD v2.0) for Wind Turbine Blades: User's Guide’, *Albuquerque, New Mexico, USA, Sandia National Laboratories, SAND2012-7028 2012.*
16. RESOR BR,2013 ‘Definition of a 5MW/61.5m Wind Turbine Blade Reference Model’, *Albuquerque, New Mexico, USA, Sandia National Laboratories, SAND2013-2569 2013.*
17. JONKMAN JM, BUTTERFIELD S, MUSIAL W, SCOTT G,2009 ‘Definition of a 5-MW Reference Wind Turbine for Offshore System Development’, *Golden, Colorado, USA, National Renewable Energy Laboratory, NREL/TP-500-38060 2009.*
18. KELLEY N, JONKMAN B,2013 ‘TurbSim’, *National Wind Technology Center, USA, v1.06.00, Last modified 30-May-2013, accessed 14-October-2013.*
19. IEC TECHNICAL COMMITTEE 88: WIND TURBINES,2005 ‘International Standard IEC 61400-1’.
20. LAINO DJ,2013 ‘AeroDyn’, *National Renewable Energy Laboratory, USA, v13.00.02a-bjj, Last modified 23-February-2013, accessed 15-October-2013.*
21. JONKMAN J,2013 ‘FAST’, *National Wind Technology Center, USA, v7.02.00d-bjj, Last modified 28-October-2013, accessed 28-October-2013.*
22. BERG JC, PAQUETTE JA, RESOR BR,2011 ‘Mapping of 1D Beam Loads to the 3D Wind Blade for Buckling Analysis’, *Collection of Technical Papers - AIAA/ASME/ASCE/AHS/ASC Structures, Structural Dynamics and Materials Conference 2011, 1-8.*
23. JENSEN FM, FALZON BG, ANKERSEN J, STANG H,2006 ‘Structural Testing and Numerical Simulation of a 34 m Composite Wind Turbine Blade’, *Composite Structures, 76, 52-61.*
24. ATAYA S, AHMED MMZ,2011 ‘Forms of Discontinuities in 100 kW and 300 kW Wind Turbine Blades’, *10th World Wind Energy Conference & Renewable Energy Exhibition 2011, 1-6.*